Surface structure of sterically stabilized ferrofluids in a normal magnetic field: Grazing-incidence x-ray study

A. Vorobiev,[1] G. Gordeev,[2] O. Konovalov,[1] and D. Orlova[2]
[1]*European Synchrotron Radiation Facility, 6 rue Jules Horowitz BP 220, 38043 Grenoble Cedex, France*
[2]*Petersburg Nuclear Physics Institute, RAS, Gatchina, St. Petersburg 188300, Russia*
(Received 22 February 2008; revised manuscript received 7 January 2009; published 19 March 2009)

We studied the internal structure of sterically stabilized water- and oil-based ferrofluids in the vicinity of the free interface with a gas by means of x-ray reflectometry and grazing-incidence x-ray diffraction. It was found that in-depth distribution of the magnetic nanoparticles in the layer close to the interface is essentially inhomogeneous. In the case of water-based ferrofluids an enhanced concentration of surfactant and subsequent reduced concentration of the particles were detected in the 100–200-Å-thick interface-adjacent layer. Scattering patterns possessing characteristic features of powder diffraction revealed partial ordering of the surfactant in a multilamellar structure. External magnetic fields applied perpendicular to the interface effectively reduced thickness of the depleted layer bringing the particles from the bulk to the surface. However no field-induced correlations between the particles were detected. In the top 500-Å-thick layer of an oil-based ferrofluid depletion of the particles density was also present; however, no special arrangement of the surfactant molecules was manifested by the experimental data. Interestingly, for all samples we observed wavy surface deformation appearing in the normal magnetic field of a strength H much smaller than the critical values H_c calculated according to the conventional theory of ferrofluid surface instability. This deformation with lateral periodicity of a few millimeters has an amplitude smoothly increasing up to a few microns at $H=0.5H_c$.

DOI: 10.1103/PhysRevE.79.031403 PACS number(s): 82.70.−y, 75.50.Mm, 61.30.Hn, 61.05.cp

I. INTRODUCTION

In ferrofluids (FFs) [1–3] magnetic nanoparticles are conventionally stabilized by a single or double layer of surface-active molecules (surfactants). Steric repulsion between surfactant shells assisted by Brownian motion prevents particle coagulation due to attractive dipole-dipole interaction. As a result, FFs behave like a stable homogeneous on *macroscopic scale* liquid magnetic media widely used for technical applications [4]. At the same time, since FF is essentially discrete system, on *micro- and nanoscales* its bulk structure can be assumed as homogeneous only if no external magnetic field is applied. In this case the particles are randomly distributed and behave like a superparamagnetic gas. Even relatively small fields break the force balance, which leads to pronounced spatial correlations between the particles that have been experimentally observed in the bulk FF in form of ordered chains [5,6], columns [7,8], and even pseudocrystalline structures [9]. These findings can reintroduce FFs as prospective materials for the modern industry based on nanotechnology.

In this context, FF ordering at the border with another material looks especially interesting because it can be applied for production of nanostructured magnetic surfaces or multilayers. Employing a FF-solid interface is one of the most straightforward way to realize this idea. Indeed, characteristics of a solid substrate governing the ordering process can be easily varied in a desired way providing different types of the resulting structures. Presumably, first experimental observation of substrate-induced FF structuring has been performed by means of a linear optic technique [10,11]. It was shown that in a FF layer wetting an optically anisotropic glass, the orientation of the magnetic particles is strongly correlated. This leads to an optical phase shift in the ordered FF layer (whose thickness is about two to four particle diameters). Interestingly, the value of the shift depended on the particle concentration, but not on the sample *p*H or size of the particles [11].

External magnetic fields applied to such kind of interfaces ought to introduce additional correlations between the FF particles and redound to further structuring of FFs. Indeed, highly ordered smecticlike multilayers have been found at the border of FF with silicon substrates by neutron scattering [12,13]. The distance between layers and their number could be controlled by the strength and direction of the external field. These experimental observations were recently supported and elucidated by molecular-dynamics simulations [14].

However, in the case of ferrofluid-solid interface the ordered FF sheet is hidden behind a substrate and its practical exploitation will require some nontrivial technological tricks. Therefore, in the present study we bring to focus an easily accessible interface of FF with gas, i.e., "free" FF surface. Indeed, if FF structure in the bulk and at the interface with solids is intrinsically different, one can expect also some peculiar ordering features on a free FF surface. Besides a general scientific interest this system appears very promising for practical applications.

In fact, investigation of the FF-gas interface morphology has twofold importance because, apart from aforesaid, studding of field-induced ordering in this system necessarily face us with a famous phenomenon of FF surface transition [15] also known as the Rosensweig instability (RI). The RI concept and main parameters are briefly depicted in the Appendix.

Optical methods were naturally used in most of experimental studies on RI starting from the moment of its discovery. Recently, a much more accurate technique—absorption

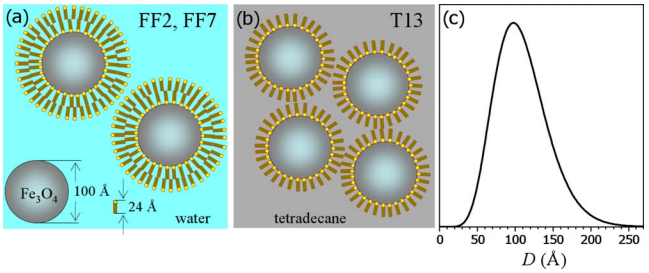

FIG. 1. (Color online) (a) Schematic presentation of magnetite nanoparticles stabilized by a double layer of sodium oleate and dispersed in water (samples FF2 and FF7). (b) The same batch of particles stabilized by a single layer of oleic acid and dispersed in tetradecane (sample T13). Size of the surfactant molecules (D_s =24 Å) and solid core (D_m=100 Å) are drawn true to scale. (c) Size distribution of the magnetic particles as obtained by TEM and x-ray diffraction.

x-ray imagining—was applied for investigation of conventional RI [16] and also for studding of RI solitons [17] and growth rate of RI undulations [18]. However, experiments with visible-light and x-ray absorptions can only bring information about the macroscopic configuration of the interface while no information about the particle organization close to it can be obtained. At the same time, surface x rays or neutron scattering—the most suitable experimental techniques—is very rarely applied [19,20].

In the present paper we report on results of our study on the particle distribution in the top FF layer adjacent to the interface with gaseous atmosphere. For this purpose specular x-ray reflectivity (XR) and grazing-incidence diffraction (GID) were used. Surface sensitivity was varied by changing the incident angle thereby defining the depth of the investigated layer from few tens to several hundreds of angstroms. A field-induced microscopic wavy deformation of the surface in subcritical fields observed in the XR experiments is also reported.

II. SAMPLES

Magnetic nanoparticles for all samples were fabricated by the chemical deposition of the dispersed magnetite Fe_3O_4 [4]. The synthesized particles were coated with surfactant, selected by weight, and dispersed in a liquid carrier by means of peptization [21]. The size distribution of the particles, obtained from the tunneling electron microscopy (TEM) and x-ray powder-diffraction measurements [22], obeys to the gamma distribution with a mean size value equal to 108 Å and dispersion of 35 Å.

In water-based samples FF2 and FF7 with volume concentration of magnetite C=2% and 7%, respectively, a double layer of sodium oleate molecules ($C_{18}H_{33}NaO_2$) was used to build surfactant protecting shell and to make the particle hydrophilic. In oil-based sample T13 with C =13 vol % a single layer of oleic acid ($C_{18}H_{33}COOH$) was used for the particle stabilization and tetradecane ($C_{14}H_{30}$) was used as a solvent. Schematic drawings of the particles and distribution of the magnetite core size D are presented in Fig. 1. Evidently, due to the thinner surfactant shell the oil-based FF remains liquid at higher volume concentration of the particles. Characteristics of the samples and constituent chemicals relevant to the present study are collected in Table I.

III. EXPERIMENT

X-ray measurements were carried out at the beamline ID10B [23] at the ESRF (Grenoble, France) with λ =1.55 Å and λ=0.56 Å. This beamline is especially designed for the grazing-incidence x-ray scattering on liquid surfaces. The FF samples were filled in a round Teflon dish of 70 mm in diameter and 5 mm deep, which was placed into a hermetic cell like that shown in Fig. 2. Inside the cell air atmosphere was replaced with humid helium to compensate water evaporation from the surface and to reduced x-ray scattering on air. Windows for incoming and scattered x-ray beams were made from Kapton film.

The sketch of the experiment is presented in Fig. 2. Ge(111) deflector crystal was used to tilt the incoming x-ray beam with respect to the FF surface, providing grazing angle α from 0° to 7°. Linear position-sensitive detector (PSD) oriented perpendicular to the surface was used to record simultaneously scattering intensity in a wide range of vertical

TABLE I. Relevant characteristics of the samples and their components. Here γ is the surface tension at 20 °C, ρ_m is the mass density, χ_i is the magnetic susceptibility in linear regime, H_c is the value of the critical field calculated according to Eq. (A1) from the Appendix, $\rho=\rho_e r_e$ is the scattering length density, ρ_e is the electron density, and r_e is the classical electron radius.

Sample or compound	γ (mN/m)	ρ_m (g/cm^3)	χ_i	H_c (Oe)	ρ (10^{-6} Å^{-2})
FF2	32	1.11	0.33	275	10.0
FF7	30	1.26	1.16	74	11.4
T13	23	1.35	2.15	36	11.6
Fe_3O_4		5.0			40.5
$C_{18}H_{33}COOH$		0.89			8.5
$C_{18}H_{33}NaO_2$	37	1.02			9.6
H_2O	72.8	1.00			9.5
$C_{14}H_{30}$	26.6	0.76			7.5

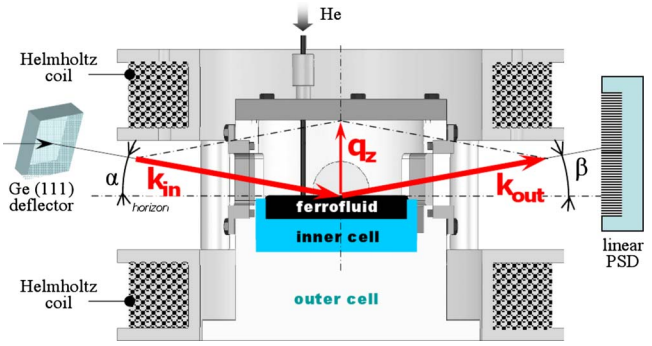

FIG. 2. (Color online) Sketch of the experiment showing the incident and reflected x-ray beams (k_{in},k_{out}) and the sample environment. Angle of scattering in horizontal plane δ is not shown.

exit angle β (up to 18°). Scattering angle in horizontal plane δ (not shown in Fig. 2) was varied during GID measurements in the range from 0° to 20°.

Normal magnetic field up to 150 Oe was created by a pair of Helmholtz coils. Field homogeneity at the sample position was better than 1%. An active antivibration device from Halcyonics [24] was used to suppress both high- and low-frequency parasitic vibrations of the sample cell coming from the neighboring equipment.

IV. SHAPE OF THE FREE FERROFLUID SURFACE: MAGNETIC FIELD EFFECT IN SUBCRITICAL REGIME

According to the conventional scenario of RI the FF free surface subjected into homogeneous magnetic field of a strength H remains flat as long as H does not overcome the critical value H_c. In terms of x-ray reflectivity experiment this means that in the field range $0<H<H_c$ FF surface behaves like a macroscopically flat liquid mirror, i.e., incoming beam impinging on the sample at the angle α sustains pure specular reflection at the exit angle β obeying the condition $\beta=\alpha$ and preserving after the interaction the same profile.

Although theoretical consideration of RI does not take into account internal structure of FF, we assumed that field-induced reorganization of the particles in the FF surface layer is possible already in subcritical fields. Existing in reality it should give rise to the effective roughening of the FF surface on a length scale suitable for observation by the grazing-incidence x-ray scattering. To check this hypothesis we measured profile and intensity of the x-ray beam reflected from air-FF7 interface during field increasing-decreasing cycles.

Unexpectedly, we found that intensity of the reflected beam and its exit angular position β smoothly deviate from their original values, which becomes visible with the naked eye already at $H\approx 0.5H_c$ (Fig. 3). At smaller α [Fig. 3(a)] the outgoing beam becomes also broader and finally splits into several low-intensity beams at $H\approx H_c$. From the condition of specular reflection $\beta=\alpha$ it evidently follows that observed increasing of β is only possible due to a relevant increasing of effective grazing angle α. Since the tilt of the incoming beam was fixed during the field scans, we conclude that the sample surface itself inclined with respect to the original horizontal plane. More surely, one can say that at least some parts of the FF surface *within the beam footprint* Φ were tilted already at $H\geq 0.5H_c$. Presumably this tilt reveals developing of the surface deformation at the early stage of RI transition.

Let us now assume reflection of a narrow x-ray beam in grazing-incidence geometry from a smooth wavelike deformation with lateral periodicity L [Fig. 3(c)]. If L is much

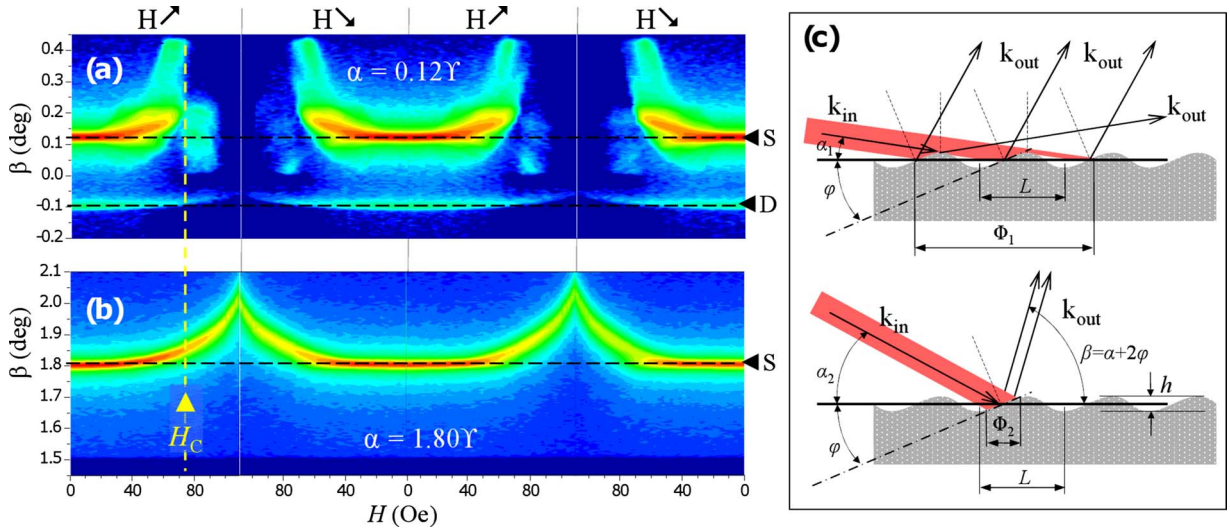

FIG. 3. (Color online) Logarithmic-scale exit-angle intensity distribution obtained for FF7 during two field increasing-decreasing cycles at grazing angle (a) $\alpha_1=0.12°$ and (b) $\alpha_2=1.80°$. Yellow dashed line indicates the value of the critical field calculated according to the conventional theory: "S" is the position of the specular beam at $H=0$ and "D" is a trace of the direct beam. (c) Schematically shown difference of specular reflection from wavy FF surface in the case of "small" (α_1) and "large" (α_2) grazing angles. Thick solid line is the horizontal plane, i.e., position of the interface at $H=0$, arrow marked k_{in} is the incoming beam and red area around indicates its vertical size of 0.1 mm, arrows marked k_{out} are reflected beams, thin dashed lines are local normals to the FF surface, φ is the local tilt angle of the deformation, L and h are lateral periodicity and amplitude of the wavy deformation, respectively, and Φ is the beam footprint.

smaller than footprint Φ the reflected beam would become broader (due to defocusing effect of curved "mirror") while its position would shift to the larger β values. In the case $L \gg \Phi$ the reflected beam would only shift without significant broadening because the sample surface within the footprint can be considered as almost flat. Therefore, from Fig. 3, where these two situations are obviously realized, one can roughly estimate characteristic size L of the humps as $\Phi_1 > L > \Phi_2$, where $\Phi_1 = 24$ mm and $\Phi_2 = 2$ mm are corresponding values of the footprint for $\alpha_1 = 0.12°$ and $\alpha_2 = 1.80°$ (note that the theoretically calculated period of standing wave L_c for this sample is 9.8 mm). Moreover, mean slope φ of the humps as a function H can also be calculated from the shift of the specular beam position as $\varphi(H) = [\beta(H) - \alpha]/2$. For example, according to Fig. 3(b) $\varphi = 0.1°$ at $H = 110$ Oe. Assuming $L = (\Phi_1 + \Phi_2)/2 = 12$ mm one can also estimate the amplitude h on the level about 10 μm.

In Fig. 3 two sequential cycles of field increasing-decreasing are shown for each α value revealing reproducible creation of surface wavy deformation in subcritical fields. This interesting observation has, however, restricted the range of the magnetic field to $H < 0.5H_c$ in the following XR and GID experiments, because these methods require very well-defined value of the grazing angle.

V. SURFACE STRUCTURE OF THE WATER-BASED FERROFLUID

In-depth structure of the FF surface was examined by means of specular x-ray reflectometry which provides information on electron density ρ_e as a function of distance z from the gas-FF interface ($z = 0$). Hereafter in the text and on related figures instead of ρ_e we use substitutive quantity scattering length density (SLD) $\rho = \rho_e r_e$, where r_e is classical electron radius.

Original exit-angle intensity distribution $I(\alpha, \beta)$ collected with a linear PSD was background corrected, normalized on intensity of the incoming beam I_0, and fitted to a model electron-density profile $\rho(z)$ using Parratt formalism [25]. The best density profile is determined by a least-squares fit analysis.

In general, deviation of the experimental reflectivity curve from Fresnel reflectivity $R_F(Q_z)$ elicits a layering process occurring at the sample surface or interface. The argument $Q_z = (4\pi/\lambda)\sin(\alpha)$ is the component of the momentum-transfer vector perpendicular to the surface (see Fig. 2). As R_F has an asymptotic Q_z^{-4}, our experimental XR data are presented in form of $R(Q_z)Q_z^4$ to compensate general decay, to give an access to the smallest features of the data, and to emphasize quality of the fit.

Retrieving the simplest $\rho(z)$ profile describing experimental data from the sample FF2 (Fig. 4) we tried, first of all, a single-layer model [black dashed line in the inset of Fig. 4(a)]. Although it allows us to repeat the main features of the experimental XR curve, some obvious discrepancies cannot be eliminated. On the other hand, three-layer model (red solid line) is already sufficient to reproduce experimental data in all details. In this model a middle sublayer is characterized by thickness $l_2 = 35$ Å and SLD value $\rho_2 = 11.8 \times 10^{-6}$ Å^{-2} which is about 20% higher than bulk value ρ_{FF2}, while neighboring layers with $l_1 \approx l_3 = 25$ Å have $\rho_1 = 0.35\rho_{FF2}$ and $\rho_3 = 0.95\rho_{FF2}$, respectively. Parameters of the very top sublayer prompt a suggestion that it is formed by the surfactant molecules staying perpendicular to the surface. First, its thickness matches the length of sodium oleate $D_s = 24$ Å. Second, the value ρ_1 is smaller than SLD of any component included in the sample FF2 (see Table I). This indicates incompleteness of the layer which is only possible in the case of small surfactant patches located on the sample surface. In much the same way we conclude that the middle sublayer l_2 is enriched with magnetite while third sublayer l_3 is slightly magnetite depleted.

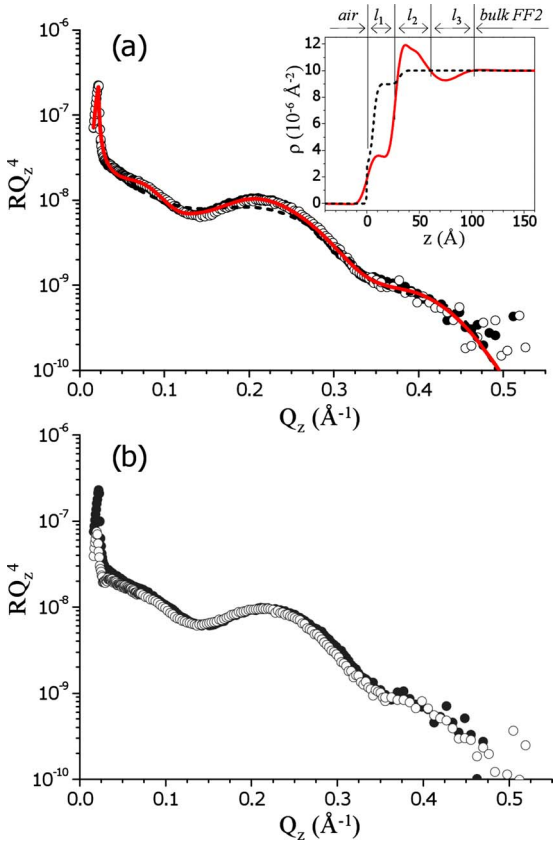

FIG. 4. (Color online) FF2 reflectivity data. (a) Time effect: filled circles correspond to 1 h after the sample assembling and open circles correspond to 9 h afterward. Black dashed line and red solid line represent fit results corresponding to the model SLD profiles shown in the inset with preservation of the line style. (b) Magnetic field effect: filled circles denote $H = 0$ and open circles denote $H = 87$ Oe ($0.3H_c$).

The described surface structure remains stable for many hours, which was confirmed by the recurrent reflectivity measurements. Specifically, experimental XR data obtained 1 and 9 h after the sample assembly coincide within statistical error [Fig. 4(a)].

The effect of the external fields on $\rho(z)$ profile is found to be negligible at least in the range $0 < H < 87$ Oe ($0.3H_c$). Field-induced difference in the XR data in low-Q_z range [Fig. 4(b)] is accounted for the macroscopic deformation of the surface described in Sec. IV.

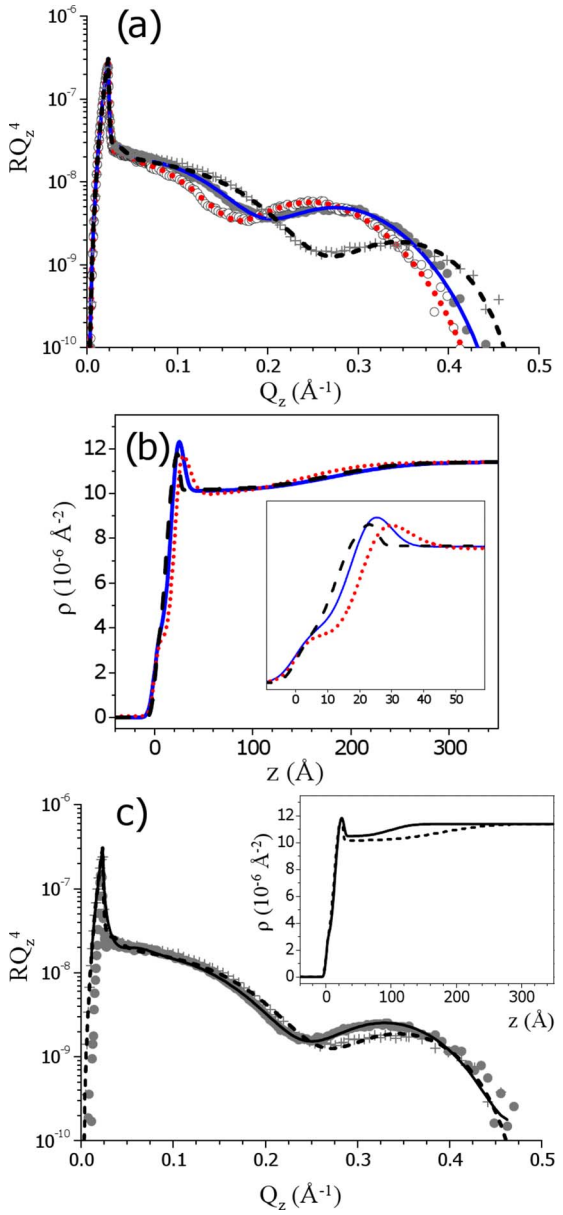

FIG. 5. (Color online) FF7 reflectivity data collation. (a) Experimental data (symbols) and fitted reflectivity curves (lines) at zero magnetic field: filled circles and blue solid line correspond to 1 h after the sample assembling, open circles and red dotted line correspond to 10 h after, and crosses and black dashed line correspond to data after surface cleaning. (b) Best model SLD profiles used to fit experimental reflectivities. Inset shows the same curves zoomed in the small-z region. (c) Effect of magnetic field after the surface cleaning: crosses and dashed line denote $H=0$ and circles and solid line denote $H=35$ Oe $(0.47H_c)$; corresponding model SLD profiles are shown in the inset.

Reflectivity curves for more concentrated water sample FF7 [Fig. 5(a)] resemble quite closely the FF2 data, indicating similar surface structure for both samples. However, results of fitting with using of the same three-layer model reveals significant quantitative difference—in the case of FF7 the thickness of third magnetite-depleted sublayer l_3 expands to 200 Å [Fig. 5(b)]. Also we observed slow $\rho(z)$ evolution in time expressed in appreciable extension of l_1 and l_2 [see inset of Fig. 5(b)].

Reproducibility of this layering process was verified by removing the upper part (a few microns thick) of the FF7 sample without touching the rest of it. Appropriate experimental data and model reflectivity are presented in Fig. 5(a) by crosses and black dashed line, respectively, while model $\rho(z)$ profile is shown by black dashed line in Fig. 5(b). One can see that recreated sublayers are very similar to the original ones; however, new l_1 and l_2 become thinner and more conjoint.

Applying of the magnetic field resulted in shrinking of the magnetite-depleted layer l_3 to 100 Å at $H=0.47H_c=35$ Oe [Fig. 5(c)]. Apparently magnetic field played a role of "stirrer" bringing more particles to the surface.

In-plane surface structure was probed by GID at different values of external magnetic field below H_c and different values of the grazing angle α. GID data were collected with linear PSD by scanning of the in-plane scattering angle δ. At the same time PSD aperture defined the range of the out-of-plane angle β. Two-dimensional distributions $I(\beta,\delta)$ were converted into momentum space and integrated over momentum modulus Q.

GID data from FF2 sample are presented in Fig. 6. Measurements were performed with $\lambda=1.55$ Å at $\alpha=0.75\alpha_c$, $\alpha=1.0\alpha_c$, and $\alpha=3.12\alpha_c$. For the highest α (i.e., at inmost penetration depth) we found several equidistant diffraction peaks at $Q_{p1}=0.123$ Å^{-1}, $Q_{p2}=0.248$ Å^{-1}, $Q_{p3}=0.373$ Å^{-1}, and $Q_{p4}=0.496$ Å^{-1} manifesting the presence of some well-defined correlation length $L_d=50.7$ Å. Whereas magnetite particles in our samples are much bigger and rather polydisperse, one supposes that such perfectly diffracting media can only be built of the surfactant molecules. Furthermore, intensity of the odd peaks $p1$ and $p3$ is higher than intensity of the even peaks $p2$ and $p4$, which implies apart from evident L_d periodicity another characteristic size $L_d/2$ which is the size of the most basic structural unit. Indeed $L_d/2$ corresponds to the length of sodium oleate molecules and we conclude that L_d is the thickness of the surfactant bilayer in which amphiphilic molecules are alternately ordered in tail-to-tail or head-to-head manner. Evidently, the bilayers are hierarchically ordered into multilayers because diffraction can only happen on periodic structures. On the other hand, in two-dimensional angular space the same data are seen as a set of complete powder-diffraction rings [Fig. 6(b)] suggesting that there is no preferential orientation of the multilayers with respect to the sample surface plane. Such situation is realized in multilamellar vesicles or micelles. In the latter case the magnetite nanoparticles originally covered with the surfactant bilayer could act as the centers of nucleation.

In the external field $H=0.2H_c=55$ Oe the diffraction features disappeared [Fig. 6(c)] demonstrating dissipation of the ordering or quantity reduction of the structured objects. However, after switching off the field the diffraction rings reverted in original state.

GID measurements on FF7 sample were performed in Q range sufficiently large to see diffraction from the nanocrystals of magnetite forming the particle cores (Fig. 7). In the case of small penetration depth $(\alpha<\alpha_c)$ no distinct diffraction features were observed (black filled circles), from which

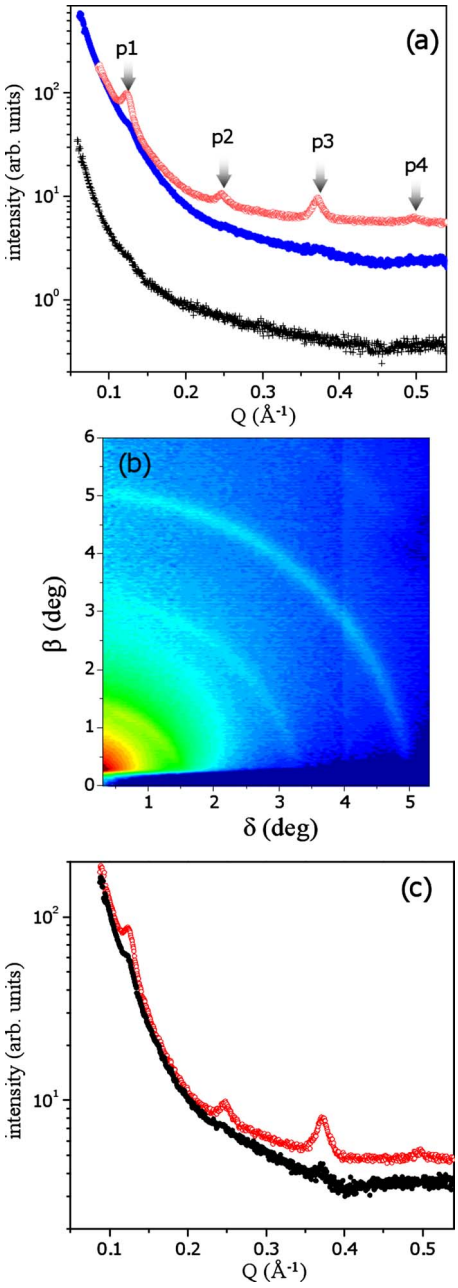

FIG. 6. (Color online) GID on FF2 sample. (a) $I(Q)$ dependence on grazing angle α at $H=0$. Black crosses: $\alpha=0.75\alpha_c$, blue filled circles: $\alpha=1.0\alpha_c$, and red open circles: $\alpha=3.12\alpha_c$. (b) 2D scattering pattern $I(\beta,\delta)$ at $\alpha=3.12\alpha_c$, $H=0$, and $\lambda=1.55$ Å. (c) Field effect at $\alpha=3.12\alpha_c$. Red open circles: $H=0$ and black filled circles: $H=0.2H_c=55$ Oe.

we conclude that the very top layer of the sample is amorphous. While at $\alpha>\alpha_c$ two groups of the diffraction peaks were detected (red open circles). The most prominent group consists of a few high-Q peaks corresponding to the crystalline structure of magnetite. This reveals the presence of the particles relatively close to the surface. In low-Q part of the same pattern one obtained two peaks analogous in position to p3 and p4 peaks for FF2 but with smaller amplitude. Interestingly, in both measurements no characteristic features of water structure factor (blue solid line) are visible, which indicates reduced concentration of water in the top layer of FF7.

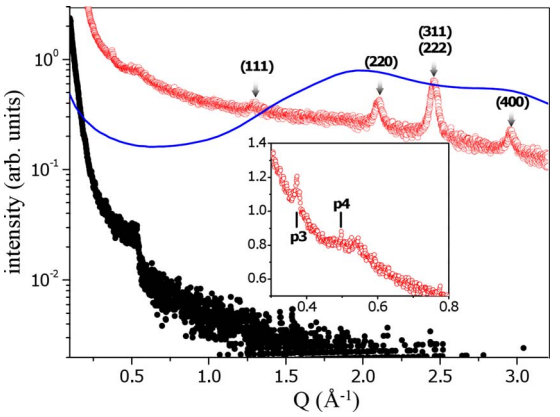

FIG. 7. (Color online) GID on FF7 at zero field. Black filled circles correspond to $\alpha=0.7\alpha_c$, red open circles denote $\alpha=1.8\alpha_c$, and blue solid line shows typical curve for pure water (measured not in the same conditions). Arrows with indices in the brackets indicate positions of the appropriate reflections from the magnetite crystal structure. In the inset low-Q part of the upper curve is zoomed in (with linear vertical scale) showing occurrence of diffraction peaks p3 and p4 identical to those obtained from the sample FF2 [see Fig. 6(a)].

VI. SURFACE STRUCTURE OF THE OIL-BASED FERROFLUID

Reflectivity data from the tetradecane ferrofluid T13 (Fig. 8) reveal a different surface structure as compared to the water samples FF2 and FF7. We noticed extremely sharp border T13-air and absence of the low-density top layer called l_1 in previous three-layer model. In T13 SLD value of a layer at $0<z<30$ Å is slightly smaller than the bulk value ρ_{T13}. The top layer is separated from the bulk by a thick ($\approx$500 Å) transition layer with a broad minimum at $z=80$ Å (where ρ corresponds to the value of pure tetrade-

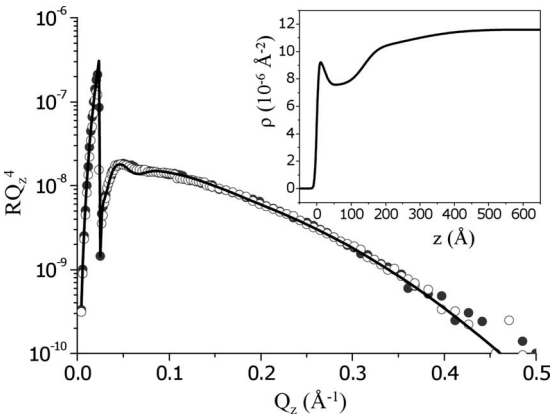

FIG. 8. Magnetic field effect on T13 reflectivity. Filled and open circles denote experimental data obtained at $H=0$ and $H=8$ Oe, respectively, and solid line represents fitted reflectivity curve corresponding to a model SLD profile shown in the inset.

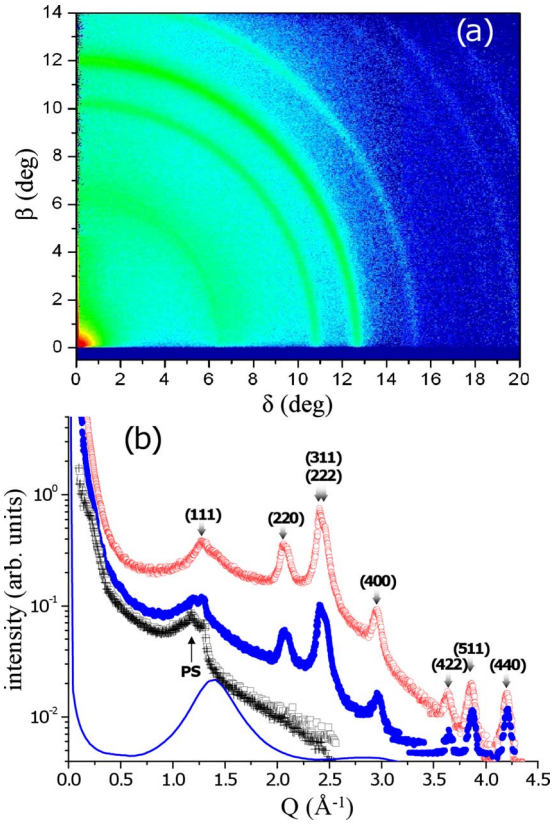

FIG. 9. (Color online) GID on T13 sample. (a) 2D scattering pattern at $\alpha=2.1\alpha_c$ and $H=10$ Oe in angular coordinates collected at $\lambda=0.56$ Å. (b) Dependence of the scattered intensity on modulus Q and grazing angle α at zero field. Gray open squires correspond to $\alpha=0.7\alpha_c$, blue filled circles to $\alpha=1.4\alpha_c$, red open circles to $\alpha=2.1\alpha_c$, black crosses to scattering on the cell windows and air without ferrofluid sample, and blue line to scattering from pure tetradecane. Arrow with "PS" label is pointing out enhanced parasitic scattering from the windows of the sample cell. Arrows with indices in the brackets indicate positions of appropriate reflections peaks from magnetite crystal structure.

cane) and asymmetric slopes—steep toward the interface and flat toward the bulk sample.

Due to the high concentration of the magnetic phase and corresponding enhanced sensitivity of T13 surface to the external fields, reflectivity data could be obtained at $H\approx 10$ Oe as maximum. No changes in the surface structure were found in this field range (Fig. 8).

GID measurements on T13 were performed in extended Q range allowing for more magnetite diffraction peaks in Fig. 9. As well as in the case of water FF magnetite peaks appear when grazing angle α exceeds the critical value (blue filled and red open circles). It was also observed a broad peak at Q values corresponding to the tetradecane structure factor (blue line). This gives a clear indication that, in contrast to the water-based samples where the solvent is substituted by the surfactant, there is significant amount of the solvent close to the surface of T13. The absence of low-Q diffraction on the ordered surfactant molecules confirms this assumption.

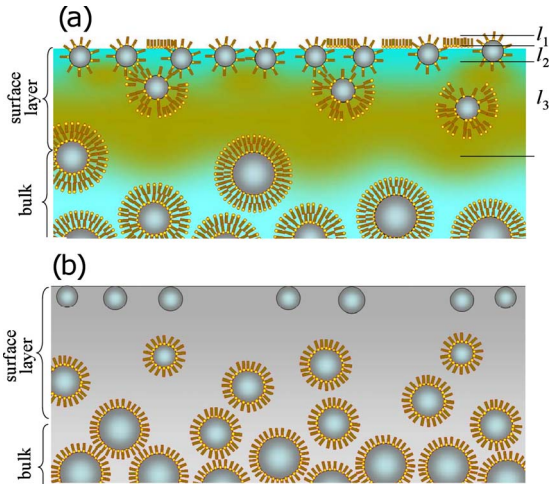

FIG. 10. (Color online) Sketch of the ferrofluid surface structure. (a) Water-based ferrofluids FF2 and FF7. Dark clouds schematically show sodium oleate molecules in the multilamellar phase. Sublayers l_1, l_2, and l_3 are described in the text. (b) Oil-based ferrofluid T13.

VII. DISCUSSION

Conjoined treatment of the XR and GID experimental data allows for considerably detailed reconstruction of the investigated interfaces FF-gas. The structure of the interface can be very different depending on the liquid carrier and type of the surfactant. Schematic arrangement of the FF surface layer for both water and oil samples are shown in Fig. 10.

In the water-based samples FF2 and FF7 the homogeneous bulk volume is covered with the surfactant-enriched layer of 100–200 Å thick. This layer, in turn, consists of three sublayers. According to the reflectivity data (Figs. 4 and 5) the topmost sublayer has thickness $l_1=25$ Å which is equal to the length of sodium oleate molecules used for the sample stabilization. For the reason that we did not observe any specific diffraction from this layer and because SLD ρ_1 is 3 times smaller than that of the compactly parked sodium oleate, we characterized l_1 sublayer as sparse and disordered. Next sublayer with $l_2=30$ Å has SLD value slightly exceeding mean bulk value. This is only possible due to the enhanced concentration of the magnetite particles since magnetite SLD is the highest in the system. Interestingly, l_2 is much smaller than mean particle size (100 Å), which indicates that only smallest particles from the whole ensemble reach the surface and stack there. This observation can be related to the problem of stabilization of the small particles with a double surfactant shell. Indeed, in the inner shell the density of the molecule tails looking toward the solvent becomes sparser with decreasing of the particle size making formation of the complete outer shell more problematic. As a result, particles covered with only one layer of sodium oleate are partially or fully hydrophobic and tend to escape from the unfriendly environment. Possibly, the single surfactant layer around "crippled" particles came to the surface can form a part of sublayer l_1 while the cores belong to l_2. Concentration of the particles in the next layer l_3 is less than in the bulk. The particles are supplanted by the surfactant which is par-

tially organized in to multilamellar blobs as it can be deduced from the characteristic diffraction patterns (Figs. 6 and 7). Layer l_3 is, however, permeable for the particles rising up when magnetic field is applied [Fig. 6(c)]. Therefore, it should be for the most part amorphous media apparently playing a role of a reservoir supplying surfactant molecules for a dynamic exchange with the particles. Described surface structure replicates several times on the same sample after surface cleaning (Fig. 6). Moreover, qualitatively the surface structure does not depend on the particle concentration (compare FF2 and FF7). That is why such kind of the top "coating" can appear an intrinsic feature of the water ferrofluids with sterically stabilized particles.

In the oil-based ferrofluid T13 the concentration of the particles smoothly increases from zero at $z=50-100$ Å (pure tetradecane layer) to the nominal bulk value at $z=500$ Å (Figs. 8 and 9). At the same time, SLD value of the topmost layer $0<z<50$ Å in T13 exceeds SLD of pure tetradecane, but it is smaller then bulk SLD of T13. Therefore, to explain this low-z peak one should, in contrast to the situation with l_2 layer in water-based samples, take into consideration three possibilities. Indeed, SLD magnitude at the peak maximum suggests that this layer could be either a complete layer of water, a close-packed layer of oleic acid, or a magnetite-enriched layer similar to l_2 in FF2 and FF7 (see Table I). Water molecules from the surrounding atmosphere could, in principle, condense on the sample. But whereas water does not wet oily surfaces, it cannot create complete 50-Å-thick layer on the top of T13. Oleic acid, used in T13 as a surfactant, dissolves perfectly in tetradecane. Although, we do not see any root for formation of a distinct oleic acid layer on the top of tetradecane, this possibility cannot be excluded for certain. However, the most realistic explanation of the SLD peak remains an enrichment of the topmost layer of T13 with magnetite in form of small particles whose density remains, nonetheless, lower than in the bulk.

One notes that SLD distributions $\rho(z)$ containing similar features have been retrieved from the x-ray reflectivity data on alkyl naphthalene ferrofluid LS-40 [19]. Interestingly, the particle-enriched layer (analog of our l_2) in LS-40 also has thickness much smaller than the mean particles size. More precisely, this thickness is equal to the smallest particle diameter obtained in LS-40 from scanning electron microscopy (SEM) measurements. Exactly the same was observed in our samples where the minimum particle size is about 30 Å [Fig. 1(c)]. This can imply an assumption about the existence of some general principles involved in the formation of the free FF surface in case of polydisperse particles.

To conclude, surfaces of water-based and oil-based FFs differ substantially from the homogeneous bulk materials. In water-based FFs surface layer has complicated structures provided by the excess of free surfactants, which seems to be unavoidable in case of polydisperse nanoparticles stabilized with a double layer of amphiphilic molecules. In oil-based FF the main feature is the gradient of the particle concentration C ranging from $C=0$ at depth $z=50-100$ Å to the nominal $C=13$ vol % at $z\geq 500$ Å. In all situations, these specific layers must govern to a great extent the value of the surface tension γ and, therefore, determine such RI parameters as the critical field H_c and the period of the standing wave L_c. On the other hand, the grade of the particle depletion in the topmost FF layer could define also the rate of the RI undulation growth with field increasing. Shrinking of the depleted layer [Fig. 5(c)] and microscopic evolution of the surface topology (Fig. 3) observed already at $H=0.5H_c$ support this hypothesis.

Apparently, x-ray reflectivity appeared as a very efficient experimental method for studding of small perturbations on the free FF surface. It allows us to measure the amplitude of the RI pattern at early stages with submicron resolution. Therefore, more systematic study such as described in Sec. IV will be continued.

ACKNOWLEDGMENTS

We gratefully acknowledge M. Mattenet (ESRF) and the staff of ID10B for technical assistance and I. Lazebnik (PNPI) and V. Zabenkin (PNPI) for fruitful discussions. One of the authors (G.G.) acknowledges Ministry of Science and Education of Russian Federation for financial support (Contract No. 02.513.11.3194).

APPENDIX: ROSENSWEIG INSTABILITY

RI is observed as a system of standing waves appearing on the surface as soon as a critical value of the magnetic field H_c is surpassed. An explanation of the FF surface transformation is based on the concept of an active response [26]: if in the homogeneous magnetic field a certain wavelike distortion arises on the FF surface then the field strength near the bulges of the perturbation will be increased (the force lines are concentrated) while near the hollows it will be decreased in comparison with the initial equilibrium state. Therefore the perturbation of magnetic force is directed upward at the bulges and downward in the hollows; it has a tendency to amplify the perturbation of the surface. This process with a positive feedback leads to the following. In the moment when continuously varying parameter H overcomes its critical value H_c, the geometry of the interface changes with a jump. At such transition, known as an exchange of stability, FF achieves a new equilibrium state. In the fields below H_c FF surface should remain flat.

In approximation of two semi-infinite media (vacuum and FF) the solution of the dispersion equation, derived in the framework of linearized perturbation and without taking into account viscosity of FF, reveals that H_c value depends on the sample mass density ρ_m, surface tension γ, magnetic susceptibility χ_i, and gravity constant g, i.e.,

$$H_c^2 = \frac{8\pi(\chi_i+2)}{\chi_i^2(\chi_i+1)}\sqrt{\rho_m \gamma g} \tag{A1}$$

and that period of the standing wave

$$L_c = 2\pi\sqrt{\gamma/\rho_m g} = 2\pi\Lambda \tag{A2}$$

does not depend on the magnetic properties of FF. Parameter Λ called capillary length demarcates the regions of domination of gravity and capillary waves. Further analysis of nonlinearized equations has allowed us to find conditions of hexagonal and cubic symmetries of the standing wave and derive its amplitude [27]. The dependence of H_c value on the viscosity and on the thickness of the sample has been also derived [28].

[1] R. E. Rosensweig, *Ferrohydrodynamics* (Cambridge University Press, Cambridge, England, 1985).
[2] E. Blums, A. Cebers, and M. M. Maiorov, *Magnetic Fluids* (de Gruyter, Berlin, 1997).
[3] *Magnetically Controllable Fluids and Their Applications*, Lecture Notes in Physics Vol. 594, edited by S. Odenbach (Springer, Berlin, 2002).
[4] B. M. Berkovsky, V. F. Medvedev, and M. S. Krakov, *Magnetic Fluids: Engineering Applications* (Oxford University Press, Oxford, 1993).
[5] M. Klokkenburg, B. H. Ernè, A. Wiedenmann, A. V. Petukhov, and A. P. Philipse, Phys. Rev. E **75**, 051408 (2007).
[6] W.-X. Fang, Z.-H. He, X.-Q. Xu, Z.-Q. Mao, and H. Shen, EPL **77**, 68004 (2007).
[7] M. Ivey, J. Liu, Y. Zhu, and S. Cutillas, Phys. Rev. E **63**, 011403 (2000).
[8] Chin-Yih Hong, Y. H. Ke, H. E. Horng, S. Y. Yang, and H. C. Yang, J. Magn. Magn. Mater. **289**, 93 (2005).
[9] A. Wiedenmann, A. Hoell, M. Kammel, and P. Boesecke, Phys. Rev. E **68**, 031203 (2003).
[10] C. Y. Matuo, A. Bourdon, A. Bee, and A. M. Figueiredo Neto, Phys. Rev. E **56**, R1310 (1997).
[11] M. Magalhães, A. M. Figueiredo Neto, A. Bee, and A. Bourdon, J. Chem. Phys. **113**, 10246 (2000).
[12] A. Vorobiev, G. Gordeev, J. Major, B. P. Toperverg, and H. Dosch, Appl. Phys. A: Mater. Sci. Process. **74**, S817 (2002).
[13] A. Vorobiev, J. Major, H. Dosch, G. Gordeev, and D. Orlova, Phys. Rev. Lett. **93**, 267203 (2004).
[14] J. Jordanovic and S. H. L. Klapp, Phys. Rev. Lett. **101**, 038302 (2008).
[15] M. D. Cowley and R. E. Rosensweig, J. Fluid Mech. **30**, 671 (1967).
[16] R. Richter and J. Bläsing, Rev. Sci. Instrum. **72**, 1729 (2001).
[17] Reinhard Richter and I. V. Barashenkov, Phys. Rev. Lett. **94**, 184503 (2005).
[18] H. Knieling, R. Richter, I. Rehberg, G. Matthies, and A. Lange, Phys. Rev. E **76**, 066301 (2007).
[19] I. Takahashi, K. Ueda, Y. Tsukahara, A. Ichimiya, and J. Harada, J. Phys.: Condens. Matter **10**, 4489 (1998).
[20] I. Takahashi, N. Tanaka, and S. Doi, J. Appl. Crystallogr. **36**, 244 (2003).
[21] E. E. Bibik, Kolloidn. Zh. **36**, 1141 (1973).
[22] A. Vorobiev, D. Chernyshov, G. Gordeev, and D. Orlova, J. Appl. Crystallogr. **41**, 831 (2008).
[23] D.-M. Smilgies, N. Boudet, B. Struth, and O. Konovalov, J. Synchrotron Radiat. **12**, 329 (2005).
[24] http://www.halcyonics.com
[25] L. G. Parratt, Phys. Rev. **95**, 359 (1954).
[26] M. I. Shliomis, Usp. Fiziol. Nauk **112**, 427 (1974).
[27] A. Gailitis, J. Fluid Mech. **82**, 401 (1977).
[28] B. Abou, G. Néron de Surgy, and J. E. Wesfreid, J. Phys. II **7**, 1159 (1997).